Catalysis Science & Technology

PAPER

View Article Online
View Journal | View Issue

Cite this: *Catal. Sci. Technol.*, 2014, **4**, 780

Molten copper hexaoxodivanadate: an efficient catalyst for SO_3 decomposition in solar thermochemical water splitting cycles†

Takahiro Kawada, Tonami Tajiri, Hiroaki Yamashita and Masato Machida*

Received 3rd November 2013,
Accepted 16th December 2013

DOI: 10.1039/c3cy00880k

www.rsc.org/catalysis

Molten copper hexaoxodivanadate (CuV_2O_6) was identified as an active catalyst for SO_3 decomposition, which is an oxygen generation step in solar thermochemical water splitting cycles, at moderate temperatures (*ca.* 600 °C). The SO_3 decomposition over CuV_2O_6 was significantly accelerated when the reaction temperature approached the melting point (*ca.* 630 °C) compared with solid phases of $Cu_2V_2O_7$ as well as other compounds in the CuO–V_2O_5 system with higher melting points (≥780 °C). A possible intermediate $CuSO_4$ species formed by SO_3 adsorption onto the Cu oxide site may decompose promptly to evolve SO_2 and O_2 on contact with the molten catalyst phase. Furthermore, the molten catalyst contained a large fraction of monovalent Cu formed by spontaneous desorption of oxygen. A possible reaction mechanism consisting of the fast dissolution of $CuSO_4$ and Cu^{2+}/Cu^{+} redox cycles in the melt is proposed.

Introduction

The large-scale production of hydrogen fuel by indirect thermochemical water splitting cycles using concentrated solar radiation as a heat source has attracted considerable attention.[1–4] Many such cycles have been proposed which rely on the decomposition of sulfuric acid as the oxygen-generating reaction.[5] One of the most promising candidates is the sulfur–iodine process, consisting of reactions (1)–(3).[5–7]

$$H_2SO_4 \rightarrow H_2O + SO_2 + 1/2O_2 \ (ca.\ 900\ ^\circ C) \quad (1)$$

$$2HI \rightarrow H_2 + I_2 \ (ca.\ 400\ ^\circ C) \quad (2)$$

$$SO_2 + I_2 + 2H_2O \rightarrow H_2SO_4 + 2HI \ (ca.\ 100\ ^\circ C) \quad (3)$$

Of these reactions, sulfuric acid decomposition (1) requires the highest reaction temperature. Sulfuric acid dissociates into H_2O and SO_3 in the gas phase above 400 °C. However, the subsequent decomposition of SO_3 into SO_2 and O_2 in the gas phase is kinetically impossible at moderate temperatures of around 600 °C, which can be achieved using conventional parabolic trough solar collectors. Therefore, economically viable catalysts which promote the slow forward reaction at or below 600 °C are crucial.

We have recently reported that copper pyrovanadate ($Cu_2V_2O_7$) is an efficient catalyst for SO_3 decomposition below 650 °C,[8] temperatures at which most conventional oxide catalysts are less active and less stable.[9–18] The combination of the pyrovanadate ($V_2O_7^{2-}$) framework, which is resistant to sulfate formation, and a copper redox species achieves both catalytic activity and stability. The catalytic activity can be enhanced by supporting the catalyst on 3-D mesoporous SiO_2 followed by thermal aging above the melting point of $Cu_2V_2O_7$ (>780 °C).[19] The thermal aging melts the $Cu_2V_2O_7$ and allows it to penetrate the mesopores of SiO_2. The simultaneous dissolution–reprecipitation of SiO_2 in the melt converts mesopores to macroporous cavities. The enhanced catalytic performance of macroporous $Cu_2V_2O_7/SiO_2$ arises from surface cavities completely covered with a thin layer of active $Cu_2V_2O_7$ and makes the catalyst an attractive alternative to Pt.[19]

These results demonstrated that melting copper vanadate opens up novel methods for preparing highly-dispersed active catalysts. In addition, the catalytic activity of the molten phase may be higher than that of the solid phase, as is the case for industrial SO_2 oxidation catalysts based on alkali metal vanadates.[20,21] Other examples of molten catalysts have been reported for partial oxidation and oxidative dehydrogenation of alkanes[22,23] and oxidation of diesel soot.[24] According to CuO–V_2O_5 phase diagrams,[25,26] CuV_2O_6, $Cu_2V_2O_7$, $Cu_3V_2O_8$, and $Cu_5V_2O_{10}$ are binary compounds. Although these three compounds with Cu/V ratios more than or equal to unity exhibit melting points above 780 °C, copper hexaoxodivanadate (CuV_2O_6)

Department of Applied Chemistry and Biochemistry, Graduate School of Science and Technology, Kumamoto University, 2-39-1 Kurokami, Chuo-ku, Kumamoto 860-8555, Japan. E-mail: machida@kumamoto-u.ac.jp; Fax: +81 96 342 3651

† Electronic supplementary information (ESI) available. See DOI: 10.1039/c3cy00880k

has the lowest melting point (*ca.* 630 °C) and may be a promising candidate as a molten catalyst for SO_3 decomposition.

We report that molten CuV_2O_6 is a highly efficient catalyst for SO_3 decomposition at or below 650 °C. Its catalytic activity and oxygen desorption properties were compared with those of our solid phase $Cu_2V_2O_7$ catalyst (m.p.: *ca.* 780 °C),[19] which does not melt at the reaction temperature. A model reaction using $CuSO_4$ as a possible intermediate was studied to elucidate the origin of the higher SO_3 decomposition activity of the molten phase compared with the solid phase.

Experimental

Preparation and characterization

Supported copper vanadate catalysts were prepared by stepwise impregnation of 3-D mesoporous SiO_2 with $Cu(NO_3)_2$ and NH_4VO_3 as described in our previous paper (see the ESI†).[19] Molar ratios of Cu : V : Si = 1 : 2 : 20 (CuV_2/SiO_2) or 1 : 1 : 20 (CuV/SiO_2) were used for the deposition of monophasic CuV_2O_6 and $Cu_2V_2O_7$, respectively.

X-ray diffraction (XRD) measurements were performed using monochromated Cu K_α radiation (30 kV, 20 mA; Multiflex, Rigaku). Raman spectra were obtained using a 532.1 nm laser excitation source (NRS-3100, Jasco). X-ray photoelectron spectroscopy (XPS) was performed using monochromated Al K_α radiation (12 keV; K-Alpha, Thermo). The Brunauer–Emmett–Teller (BET) surface area and pore volume of the as-prepared catalysts were determined from N_2 adsorption–desorption isotherms measured at 77 K (Belsorp mini, Bel Japan).

Catalytic reactions

The catalytic reaction was carried out in a quartz tubular flow reactor (ESI,† Fig. S1) as described in our previous paper.[19] Sulfuric acid (95%) was pumped (50 μL min^{-1}) and vaporized at 450 °C in a flow of N_2 (100 cm^3 min^{-1}) and thermally decomposed into SO_3 and H_2O at 600 °C. The gas mixture of 14% SO_3, 18% H_2O, and N_2 balance (WHSV = 55.2 g-H_2SO_4 (g-cat)$^{-1}$ h^{-1}) was supplied to a catalyst bed (≥600 °C). The conversion of SO_3 to SO_2 was calculated from the O_2 concentration downstream of the catalyst bed using a magneto-pneumatic oxygen analyzer (MPA3000, Horiba) and a gas chromatograph (GC8A, Shimadzu) fitted with a MS-5A column and a thermal conductivity detector. He was used as the carrier. The SO_2 concentration in the effluent gas was also determined using iodimetric titration.

Temperature-programmed desorption of oxygen (O_2-TPD) from CuV_2O_6 and $Cu_2V_2O_7$ was measured in a conventional flow reactor. Prior to the measurements, the sample was treated under a flow of 20 vol% O_2/He at 500 °C for 1 h. After cooling and evacuation, the sample was heated from ambient temperature to the melting temperature at a constant rate of 10 °C min^{-1} in a flow of He. The gas leaving the sample was analyzed using an online quadrupole mass spectrometer (Omnistar, Pfeiffer).

The thermal decomposition behavior of $CuSO_4$ and a $CuSO_4$–CuV_2O_6 mixture in a He flow was determined by thermogravimetry-differential thermal analysis coupled with evolved gas analysis using mass spectrometry (TG-DTA-MS) (20 °C min^{-1}; ThermoMass, Rigaku). The evolved gases were introduced directly to the MS ion source using a skimmer interface system without condensation or further reactions.[27] Quantitative evolved gas analysis was carried out using a non-diffusive infrared (NDIR) SO_2 analyzer and a magneto-pneumatic O_2 analyzer (MPA) (VA3000, Horiba). The evolved SO_3 was removed from the stream before gas analyses by using an adsorbent (MC050A, Horiba) to protect the detectors.

Results and discussion

Catalytic activity for SO_3 decomposition

Table 1 summarizes the physicochemical properties of CuV_2/SiO_2 (Cu : V : Si = 1 : 2 : 20) and CuV/SiO_2 (Cu : V : Si = 1 : 1 : 20). The deposition of CuV_2O_6 and $Cu_2V_2O_7$ on the as-prepared catalysts, CuV_2/SiO_2 and CuV/SiO_2, respectively, was verified by Raman spectroscopy (ESI,† Fig. S2). Because the BET surface area and the pore volume of as-prepared catalysts are comparable, their effect on catalytic activity would be negligible. The Cu and V loadings used in this study were less than those used in our previous work (Cu : V : Si = 1 : 1 : 15)[19] to evaluate the catalytic activity under kinetic control.

Fig. 1 shows the evolution of SO_3 conversion over two types of catalysts *versus* time during stepwise changes of the reaction temperature. Although the activity of both catalysts increased with increasing temperature from 600 to 750 °C, their time-on-stream behaviors at 650 °C were different. In contrast to the stable but low SO_3 conversion (<1.5%) over CuV/SiO_2 (Fig. 1b), the conversion for CuV_2/SiO_2 increased with time-on-stream (Fig. 1a) and achieved a twenty-fold higher value (>25%) than that for CuV/SiO_2. The higher SO_3 conversion for CuV_2/SiO_2 suggests that the intrinsic activity of CuV_2O_6 is higher than that of $Cu_2V_2O_7$. Furthermore, the catalytic activity was accelerated when the reaction temperature reached the melting point of CuV_2O_6 (*ca.* 630 °C). In contrast, CuV/SiO_2 remained in a solid state because of the higher melting point of $Cu_2V_2O_7$ (780 °C). Steady-state SO_3 conversions for each catalyst are shown in the ESI† (Fig. S3). Other Cu–V oxides with higher melting points ($Cu_3V_2O_8$ and $Cu_5V_2O_{10}$) were less active than $Cu_2V_2O_7$.[8]

Although CuV_2/SiO_2 initially showed some activity at 600 °C, this activity declined after a short time (Fig. 1a). The structural changes in CuV_2O_6 during this period were studied by Raman spectroscopy (ESI,† Fig. S4). After the catalytic reaction, bands corresponding to the solid CuV_2O_6 phase became weak and new bands corresponding to the sulfate (SO_4) appeared, suggesting a reaction between SO_3 and the Cu oxide species on the catalyst surface. Thermodynamic calculations predict that the formation of $CuSO_4$ ($CuO + SO_3 \rightarrow CuSO_4$, $\Delta G° = -57$ kJ mol^{-1}) is more favorable at 600 °C than the formation of $VOSO_4$ ($1/2V_2O_5 + SO_3 \rightarrow VOSO_4 + 1/4O_2$, $\Delta G° = -5$ kJ mol^{-1}). Considering that $CuSO_4$ is an intermediate species in SO_3 decomposition over molten CuV_2/SiO_2, its thermal behavior should help elucidate the cause of the accelerated SO_3 decomposition at the melting point of CuV_2O_6.

Table 1 Physicochemical properties of supported Cu–V catalysts

Catalyst	Molar ratio Cu : V : Si	Cu–V phase (m.p./°C)	S_{BET}[a]/m^2 g^{-1}	Pore volume[a]/cm^3 g^{-1}
CuV_2/SiO_2	1 : 2 : 20	CuV_2O_6 (630 °C)	463	0.74
CuV/SiO_2	1 : 1 : 20	$Cu_2V_2O_7$ (780 °C)	485	0.72

[a] BET surface area and pore volume after calcination at 600 °C.

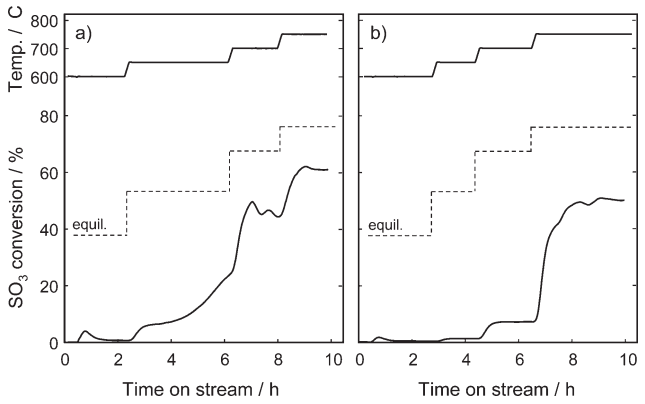

Fig. 1 Catalytic SO_3 conversion over a) CuV_2/SiO_2 and b) CuV/SiO_2 *versus* time-on-stream during stepwise changes in reaction temperature. Equilibrium conversions are shown as dashed lines.

Thermal behavior of $CuSO_4$

We studied the thermal behavior of a physical mixture of $CuSO_4$–CuV_2O_6 (1 : 1 molar ratio) as a model system by TG-DTA-MS. Fig. 2 compares the results for pure $CuSO_4$ and a $CuSO_4$–CuV_2O_6 mixture during heating in a He flow. When $CuSO_4$ was heated, sulfate decomposition occurred at around 550 °C. Double peaks in the DTA and gas evolution profiles suggest that the decomposition takes place in two steps *via* an oxysulfate.

$$CuSO_4 \rightarrow 0.5CuO{\cdot}CuSO_4 \rightarrow CuO \quad (4)$$

In the MS spectra, signals for m/z = 64 (SO_2), 48 (SO fragment, not shown), and 32 (O_2) were detected, but the signal at m/z = 80 (SO_3) was negligible. The parallel quantitative gas analysis results are summarized in Table 2. The amounts of SO_2 and O_2 evolution normalized by the amount of SO_4 in the solid suggest the occurrence of stoichiometric reaction (5).

$$CuSO_4 \rightarrow CuO + SO_2 + 1/2O_2 \quad (5)$$

The $CuSO_4$–CuV_2O_6 mixture also underwent decomposition at around 550 °C (Fig. 2b), although a very steep increase in the mass signals at m/z = 64 and 32 was accompanied by rapid weight loss at 630 °C, where melting of CuV_2O_6 produced a sharp endothermic peak. The intensity of mass signals indicated that the maximum rate of decomposition for $CuSO_4$–CuV_2O_6 is more than six-fold that of $CuSO_4$ alone. The amount of evolved gases in Table 2 also shows an amount of SO_2 nearly equivalent to the amount of SO_4 in the solid, which demonstrates almost complete decomposition of $CuSO_4$ as shown in (5), although excess O_2 in the evolved gas ($SO_2 : O_2$ = 0.95 : 0.71) results from oxygen desorption from CuV_2O_6. These results suggest that the decomposition of $CuSO_4$ to evolve SO_2/O_2 is significantly accelerated in contact with the molten CuV_2O_6 catalyst.

To clarify why molten CuV_2O_6 promotes sulfate decomposition to SO_2/O_2, the $CuSO_4$–CuV_2O_6 mixture was characterized from the Raman spectra after a temperature ramp to 600 and 630 °C at 10 °C min^{-1} and subsequent rapid cooling to ambient temperature in a flow of N_2 (Fig. 3). The as-prepared mixture (a) showed the CuV_2O_6 bands, ν(VO) (906 cm^{-1}), ν(VOV) (791, 712 and 512 cm^{-1}), and δ(OVO) (434 cm^{-1}), and the $CuSO_4$ bands, $\nu(SO_4)$ (1005 and 980 cm^{-1}). The CuV_2O_6 bands indicate that the crystal structure of CuV_2O_6 consisted of distorted octahedral VO_6.[28] Heating at 600 °C, just below the melting point of CuV_2O_6, significantly weakened the $CuSO_4$ bands and yielded several new bands (b). The bands indicated with circles at 930, 915, 856, and 501 cm^{-1} were attributed to stretching and bending modes of tetrahedral VO_4 in an infinite-chain arrangement,[29] whereas those with asterisks at 1150–1200, 1056, 605, and 458 cm^{-1} belong to stretching and bending modes of tetrahedral SO_4. This shows that the structural transformation from octahedral VO_6 in CuV_2O_6 to tetrahedral VO_4 in the melt is in progress. Tetrahedral VO_4 is the predominant coordination polyhedron in many melts containing V_2O_5.[30–33] Another set of bands corresponding to tetrahedral SO_4 probably arose from the oxysulfate ($CuO{\cdot}CuSO_4$) coming into contact with the melt. Therefore, the molten phase was composed of VO_4 and SO_4 units. Finally, the SO_4 Raman bands disappeared as soon as the temperature reached 630 °C (c), where a sharp endothermic peak was observed (Fig. 2b). The sudden disappearance of sulfate at 630 °C, where CuV_2O_6 melts, is consistent with the sudden evolution of SO_2 and O_2 in Fig. 2b.

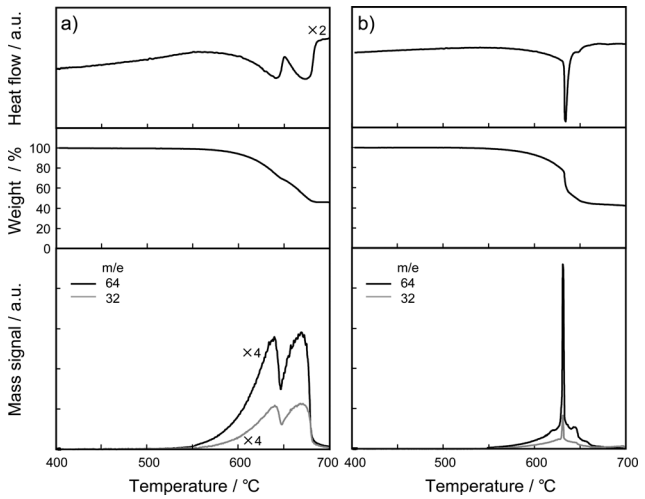

Fig. 2 TG-DTA-MS profiles for a) $CuSO_4$ and b) $CuSO_4$–CuV_2O_6 measured at a heating rate of 20 °C min^{-1} in a flow of He. The data are normalized by the unit amount of $CuSO_4$.

Table 2 Evolved gas analysis for thermal decomposition of $CuSO_4$

	SO_4 in solid/mol	SO_2 evolved[a]/mol	O_2 evolved[b]/mol
$CuSO_4$	1.00	1.01	0.47
$CuSO_4 + CuV_2O_6$	1.00	0.95	0.71

[a] Determined using a NDIR SO_2 analyzer. [b] Determined using a magnetopneumatic O_2 analyzer.

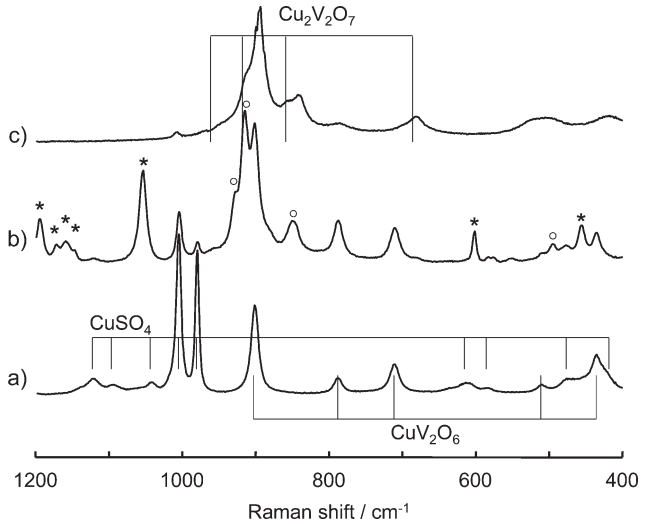

Fig. 3 Raman spectra of $CuSO_4$–CuV_2O_6 a) before heating and after heating at b) 600 °C and c) 630 °C in a flow of N_2 followed by rapid cooling to ambient temperature. Bands indicated by circles and asterisks are assigned to tetrahedral VO_4 and SO_4, respectively.

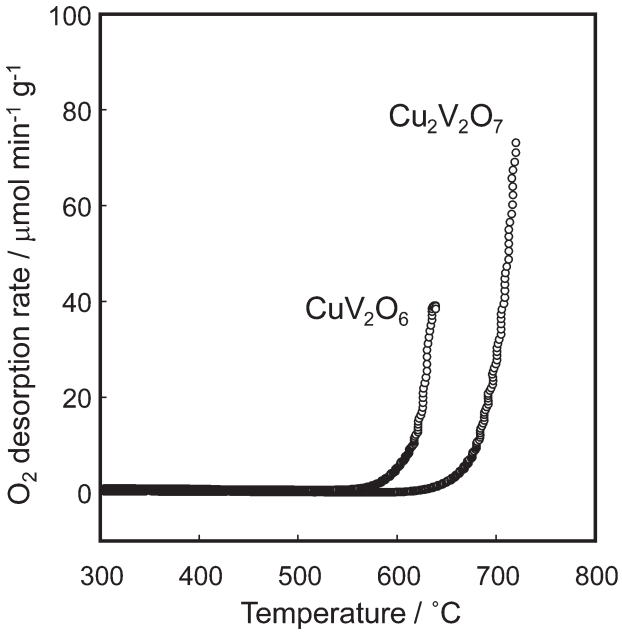

Fig. 4 Temperature programmed desorption of O_2 from CuV_2O_6 and $Cu_2V_2O_7$ in a flow of He. Heating rate: 10 °C min^{-1}.

The sulfate species dissolved in the melting vanadate is thus probably responsible for the efficient SO_3 decomposition in Fig. 1a.

In the Raman spectrum after heating at 630 °C, the bands due to $Cu_2V_2O_7$ appeared in addition to CuV_2O_6 bands (Fig. 3c). According to the phase diagram of CuO–V_2O_5,[26] incongruent melting of CuV_2O_6 yields a solid phase ($Cu_2V_2O_7$) and a liquid phase with a Cu/V ratio of less than 0.5, which solidifies as CuV_2O_6 and V_2O_5. However, because immediate solid-state reactions between $Cu_2V_2O_7$ and V_2O_5 produce CuV_2O_6, it appears to behave just like congruent melting.

Proposed mechanism for catalysis by molten CuV_2O_6

According to the reaction scheme firstly proposed by Tagawa and a co-worker,[17] SO_3 decomposition over metal oxide catalysts proceeds *via* a sulfate intermediate.

$$MO + SO_3 \rightarrow (MSO_4) \rightarrow MO_2 + SO_2 \quad (6)$$

$$MO_2 \rightarrow MO + 1/2O_2 \quad (7)$$

This reaction scheme suggests that the oxygen removal after desorption of SO_2 is a key step for the SO_3 decomposition. Fig. 4 compares O_2-TPD profiles of unsupported CuV_2O_6 and $Cu_2V_2O_7$. Although both materials desorbed a considerable amount of O_2 above 550 °C, CuV_2O_6 exhibited much faster O_2 desorption than did $Cu_2V_2O_7$. Fig. 5 shows the Cu2p and V2p XPS spectra of CuV_2O_6 before and after O_2-TPD measurements up to 600 °C. The V2p spectra consisting of a single V^{5+} peak remain unchanged after O_2 desorption. By contrast, the Cu2p spectra show the presence of Cu^+ in addition to Cu^{2+} even for the as-prepared sample after calcination in air. This means that the surface of CuV_2O_6 is easily reducible. The monovalent

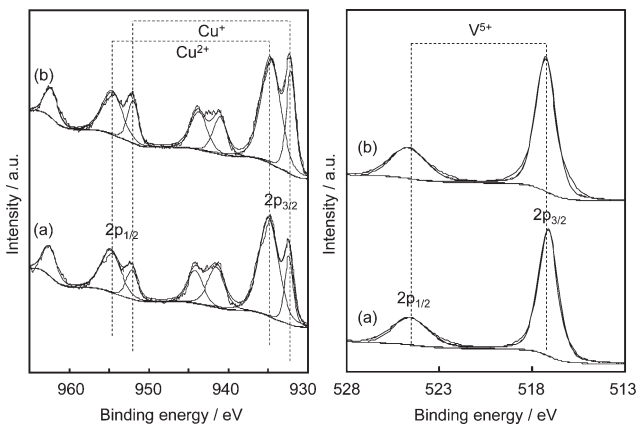

Fig. 5 Cu2p and V2p XPS spectra of CuV_2O_6 a) before and b) after O_2-TPD measurements up to 600 °C (Fig. 4).

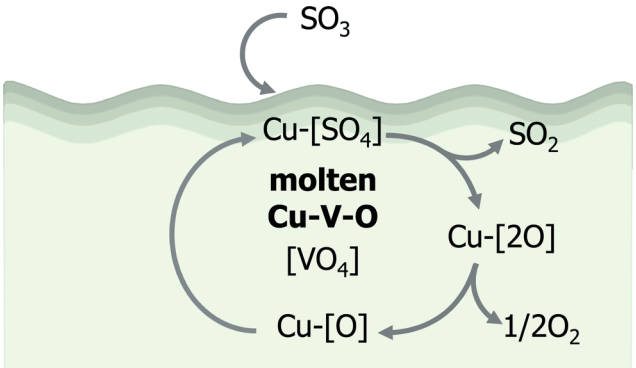

Fig. 6 Proposed reaction mechanism for SO_3 decomposition over a supported molten CuV_2O_6 catalyst.

copper increased after O_2-TPD measurements from 25% Cu^+/75% Cu^{2+} to 50% Cu^+/50% Cu^{2+}, suggesting that the spontaneous O_2 release in Fig. 4 is the result of elimination of lattice oxygen accompanied by Cu^{2+} reduction to Cu^+. It is noteworthy that the O_2 release from CuV_2O_6 increased rapidly when approaching the melting point (*ca.* 630 °C). This means that the molten phase of CuV_2O_6 contains a considerable amount of monovalent Cu, the proportion of which reached 100% at 650 °C as determined by thermogravimetric analysis (ESI,† Fig. S5).

Fig. 6 shows our proposed mechanism for the accelerated catalytic SO_3 decomposition over the supported molten copper vanadate catalyst. On the surface of the molten vanadate, SO_3 adsorption to Cu oxide species produces $CuSO_4$ species because it is thermodynamically favored around 600 °C. Here, one important contribution of the liquid surface to the catalytic reaction is the dissolution of the Cu[SO_4] species in the molten phase, leaving the liquid surface with more vacant sites for further SO_3 adsorption. Because the molten phase consists of tetrahedral VO_4 and Cu^+, the dissolved [SO_4] is immediately reduced to evolve SO_2 and then the reoxidized Cu^{2+} oxides, Cu[2O], release oxygen. The resulting free monovalent copper oxide species, Cu[O], defuses back to the liquid surface, where its reaction with SO_3 forms Cu[SO_4] again. In this way, the molten copper vanadate enables fast cycles of SO_3 capture and decomposition to SO_2/O_2. This reaction mechanism is quite different from well-known molten salt catalysts for industrial SO_2 oxidation. In SO_2 oxidation over molten V_2O_5 catalysts containing alkali metals, several vanadium oxosulfato complexes are proposed as catalytically active species.[20,34] Although these complexes were not observed in our system, analogy to SO_2 oxidation catalysts implies that interactions between molten Cu vanadate and SO_4 play a key role in SO_3 decomposition. Further attempts to identify the catalytically active species in the SO_3 decomposition are in progress.

Conclusions

We demonstrated that molten CuV_2O_6 is an efficient catalyst for SO_3 decomposition at moderate temperatures. The molten CuV_2O_6 is capable of decomposing the $CuSO_4$ species, which is a possible intermediate formed by SO_3 adsorption to Cu oxide species on the surface of the molten catalyst. Unlike solid surfaces, the molten catalyst surface enables quick regeneration of the SO_3 adsorption sites by dissolving the $CuSO_4$ species in the melt. The molten phase also enables spontaneous desorption of oxygen and thus the generation of monovalent Cu, which accelerates the decomposition of SO_3 to SO_2. The proposed mechanism provides a new strategy for designing efficient catalyst materials for SO_3 decomposition at moderate temperatures, which is a key requirement for solar thermochemical hydrogen production.

Acknowledgements

This work was supported by JSPS KAKENHI grant number 24246130 and by the Energy Carrier Project of JST ALCA (Japan Science and Technology Agency – Advanced Low Carbon Technology Research and Development Program).

Notes and references

1 S. Brutti, G. De Maria, G. Cerri, A. Giovannelli, B. Brunetti, P. Cafarelli, V. Barbarossa and A. Ceroli, *Ind. Eng. Chem. Res.*, 2007, **46**, 6393–6400.
2 J. E. Funk, *Int. J. Hydrogen Energy*, 2001, **26**, 185–190.
3 A. Meyer, J. Ganz and A. Steinfeld, *Chem. Eng. Sci.*, 1996, **51**, 3181.
4 A. Steinfeld, *Sol. Energy*, 2005, **78**, 603–615.
5 D. R. O'Keefe, J. H. Norman and D. G. Williamson, *Catal. Rev.: Sci. Eng.*, 1980, **22**, 325–369.
6 M. Dokiya, T. Kameyama, K. Fukuda and Y. Kotera, *Bull. Chem. Soc. Jpn.*, 1977, **50**, 2657–2660.
7 D. O'Keefe, C. Allen, G. Besenbruch, L. Brown, J. Norman, R. Sharp and K. McCorkle, *Int. J. Hydrogen Energy*, 1982, **7**, 381–392.
8 M. Machida, Y. Miyazaki, Y. Matsunaga and K. Ikeue, *Chem. Commun.*, 2011, **47**, 9591–9593.
9 H. Abimanyu, K. D. Jung, K. W. Jun, J. Kim and K. S. Yoo, *Appl. Catal., A*, 2008, **343**, 134–141.
10 A. M. Banerjee, M. R. Pai, S. S. Meena, A. K. Tripathi and S. R. Bharadwaj, *Int. J. Hydrogen Energy*, 2011, **36**, 4768–4780.
11 V. Barbarossa, S. Brutti, B. Brunetti, M. Diamanti and G. Ricci, *Ind. Eng. Chem. Res.*, 2009, **48**, 625–631.
12 R. D. Brittain and D. L. Hildenbrand, *J. Phys. Chem.*, 1983, **87**, 3713–3717.
13 A. Giaconia, S. Sau, C. Felici, P. Tarquini, G. Karagiannakis, C. Pagkoura, C. Agrafiotis, A. G. Konstandopoulos, D. Thomey, L. de Oliveira, M. Roeb and C. Sattler, *Int. J. Hydrogen Energy*, 2011, **36**, 6496–6509.
14 D. M. Ginosar, H. W. Rollins, L. M. Petkovic and K. C. Burch, *Int. J. Hydrogen Energy*, 2009, **34**, 4065–4073.
15 G. Karagiannakis, C. C. Agrafiotis, A. Zygogianni, C. Pagkoura and A. G. Konstandopoulos, *Int. J. Hydrogen Energy*, 2011, **36**, 2831–2844.

16 T. H. Kim, G. T. Gong, B. G. Lee, K. Y. Lee, H. Y. Jeon, C. H. Shin, H. Kim and K. D. Jung, *Appl. Catal., A*, 2006, **305**, 39–45.
17 H. Tagawa and T. Endo, *Int. J. Hydrogen Energy*, 1989, **14**, 11–17.
18 L. N. Yannopoulos and J. F. Pierre, *Int. J. Hydrogen Energy*, 1984, **9**, 383.
19 M. Machida, T. Kawada, S. Hebishima, S. Hinokuma and S. Takeshima, *Chem. Mater.*, 2012, **24**, 557–561.
20 A. Christodoulakis and S. Boghosian, *J. Catal.*, 2003, **215**, 139–150.
21 O. B. Lapina, B. S. Bal'zhinimaev, S. Boghosian, K. M. Eriksen and R. Fehrmann, *Catal. Today*, 1999, **51**, 469–479.
22 J. B. Branco, G. Lopes, A. C. Ferreira and J. P. Leal, *J. Mol. Liq.*, 2012, **171**, 1–5.
23 C. P. Kumar, S. Gaab, T. E. Müller and J. A. Lercher, *Top. Catal.*, 2008, **50**, 156–167.
24 S. J. Jelles, B. A. A. L. Van Setten, M. Makkee and J. A. Moulijn, *Appl. Catal., B*, 1999, **21**, 35–49.
25 P. Fleury, *C. R. Seances Acad. Sci., Ser. C*, 1966, **263**, 1375–1377.
26 V. Cirilli, A. Burdese and C. Brisi, *Atti Accad. Sci. Torino, Cl. Sci. Fis., Mat. Nat.*, 1961, **95**, 197–228.
27 T. Tsugoshi, T. Nagaoka, K. Hino, T. Arii, M. Inoue, Y. Shiokawa and K. Watari, *J. Therm. Anal. Calorim.*, 2005, **80**, 787–789.
28 C. Calvo and D. Manolescu, *Acta Crystallogr., Sect. B: Struct. Crystallogr. Cryst. Chem.*, 1973, **29**, 1743–1745.
29 S. Onodera and Y. Ikegami, *Inorg. Chem.*, 1980, **19**, 615–618.
30 S. Takeda, Y. Kawakita, M. Inui, K. Maruyama, S. Tamaki, K. Sugiyama and Y. Waseda, *J. Non-Cryst. Solids*, 1996, **205–207**, 151–154, Part 1.
31 S. Kaoua, S. Krimi, A. El Jazouli, E. K. Hlil and D. de Waal, *J. Alloys Compd.*, 2007, **429**, 276–279.
32 D. Maniu, I. Ardelean and T. Iliescu, *Mater. Lett.*, 1995, **25**, 147–149.
33 H. Li, H. Lin, W. Chen and L. Luo, *J. Non-Cryst. Solids*, 2006, **352**, 3069–3073.
34 S. Boghosian, A. Chrissanthopoulos and R. Fehrmann, *J. Phys. Chem. B*, 2001, **106**, 49–56.